energies

MDPI

Article

Inelastic Material Models of Type 316H for Elevated Temperature Design of Advanced High Temperature Reactors

Gyeong-Hoi Koo * and Ji-Hyun Yoon

Korea Atomic Energy Research Institute, Daejeon 34057, Korea; jhyoon4@kaeri.re.kr
* Correspondence: ghkoo@kaeri.re.kr; Tel.: +82-42-868-2950

Received: 22 July 2020; Accepted: 2 September 2020; Published: 2 September 2020

Abstract: In this paper, the inelastic material models for Type 316H stainless steel, which is one of the principal candidate materials for elevated temperature design of the advanced high temperature reactors (HTRs) pressure retained components, are investigated and the required material parameters are identified to be used for both elasto-plastic models and unified viscoplastic models. In the constitutive equations of the inelastic material models, the kinematic hardening behavior is expressed with the Chaboche model with three backstresses, and the isotropic hardening behavior is expressed by the Voce model. The required number of material parameters is minimized to be ten in total. For the unified viscoplastic model, which can express both the time-independent plastic behavior and the time-dependent viscous behavior, the constitutive equations have the same kinematic and isotropic hardening parameters of the elasto-plastic material model with two additional viscous parameters. To identify the material parameters required for these constitutive equations, various uniaxial tests were carried out at isothermal conditions at room temperature and an elevated temperature range of 425–650 °C. The identified inelastic material parameters were validated through the comparison between tests and calculations.

Keywords: Type 316H; inelastic material model; material parameter; elasto-plastic; viscoplastic; elevated temperature; nuclear power; kinematic hardening; isotropic hardening

1. Introduction

One of main issues in the development of advanced high temperature reactors (HTRs), such as sodium-cooled fast reactors, molten salt-cooled reactors, lead or lead-bismuth-cooled reactors, and high or very high temperature gas-cooled reactors, is to develop design materials applicable for elevated temperature services with long life times over 60 years.

In elevated temperature design, the strain or deformation-based design is important because structural failure modes are deeply related to a large accumulated plastic strain, creep strain, creep rupture, and creep-fatigue damage. To assure structural integrity against such damages in an elevated temperature design, an inelastic analysis approach, using accurate material models, can be a powerful tool to be able to eliminate excessive conservatism contained in design acceptance criteria on current nuclear codes and standards.

The codes and standards as rules or guidelines applicable for the elevated temperature design of the HTRs are ASME-Division 5 [1], RCC-MRx [2], Monju design guide [3], and R5 [4]. Current ASME BPVC Section III, Division 5 provides five design materials for Class A (Safety-related) components, such as Type 304SS, Type 316H, Alloy800H, 2(1/4)Cr-1Mo, and 9Cr-1Mo-V. Recently, Alloy 617 was newly included to be used for Class A components in elevated temperature services [5]. Among the allowed design materials, Type 316H is mainly considered to be used for the design of component

vessels and internals, due to its outstanding material performance in elevated temperature service. As for the same usage of ASME Type 316H stainless steel in elevated temperature services for HTRs, RCC-MRx, and Monju Design Guide provide Type 316LN stainless steel [6].

There have been many studies for Type 316H stainless steel [7–14]. However, the published material data of Type 316H are not enough for the inelastic material models to be used for the elevated temperature design of HTRs. They mainly investigate the time dependent material behavior focused on the creep or stress relaxation behavior at specific temperatures. For the purpose of the elevated temperature design by the inelastic analysis method, the inelastic material models should be able to express time-independent cyclic material behavior and time-dependent viscous behavior to cover all design temperature ranges of the HTRs. There have been studies with the same purpose for 9Cr-1Mo-V steel [15,16], which is one of the allowed Class A design materials in ASME-Division 5.

In this paper, the inelastic material models for Type 316H, which is one of principal candidate materials for the elevated temperature design of the HTRs components, is investigated and the required number of material parameters is simplified to be ten for the elasto-plastic model and to use additional two for the unified viscoplastic model. In the constitutive equations of the inelastic material models, the kinematic hardening behavior is expressed with the Chaboche model with three backstresses [17–19] and the isotropic hardening behavior is expressed by simplifying the Voce model [19]. To identify the material parameters required for these constitutive equations, various tests are carried out at isothermal conditions of a room temperature and elevated temperature range of 425–650 °C. The identified inelastic material parameters are validated through the comparison between tests and calculations.

2. Inelastic Material Models

2.1. Elasto-Plastic Model

The total strain increment tensor can be expressed as the sum of the elastic and plastic strain increment tensors as follows;

$$\dot{\varepsilon}_{ij} = \dot{\varepsilon}^{e}_{ij} + \dot{\varepsilon}^{p}_{ij} \tag{1}$$

In above, the elastic strain tensor is obtained by differentiating the elastic potential function with respect to the stress tensor σ_{ij}. As the same way, the plastic flow equations are obtained from the yield function $f(\sigma_{ij})$, which is a scalar function of the stresses, as follows;

$$\dot{\varepsilon}^{p}_{ij} = \lambda \frac{\partial f}{\partial \sigma_{ij}} \tag{2}$$

where λ is a positive scale factor of proportionality having zero in the elastic domain. It can be derived as follows;

$$\lambda = \frac{1}{H}\left\langle \frac{\partial f}{\partial \sigma_{ij}} \dot{\sigma}_{ij} \right\rangle \tag{3}$$

In above, H is a plastic modulus and $< >$ indicates the MacCauley bracket.

The yield function, f and the plastic modulus, H in Equations (2) and (3) are expressed as follows [15]:

$$f\left(\sigma_{ij} - a_{ij}\right) = \sqrt{\frac{3}{2}\left(\tau_{ij} - \alpha_{ij}\right)\left(\tau_{ij} - \alpha_{ij}\right)} - \sigma_{yo} - R = 0 \tag{4}$$

$$H = E_{ijkl}\frac{\partial f}{\partial \sigma_{ij}}\frac{\partial f}{\partial \sigma_{kl}} + \frac{2}{3}\sum_{k=1}^{n}(C_k)\frac{\partial f}{\partial \sigma_{ij}}\frac{\partial f}{\partial \sigma_{ij}} - \sum_{k=1}^{n}\left[\gamma_k(\alpha_{ij})_k\right]\frac{\partial f}{\partial \sigma_{ij}}\sqrt{\frac{2}{3}\frac{\partial f}{\partial \sigma_{kl}}\frac{\partial f}{\partial \sigma_{kl}}} + b(Q-R)\sqrt{\frac{2}{3}\frac{\partial f}{\partial \sigma_{mn}}\frac{\partial f}{\partial \sigma_{mn}}} \tag{5}$$

where τ_{ij}, a_{ij}, and α_{ij} indicate deviatoric stress tensor, total backstress tensor, and deviatoric backstress tensor, respectively. R and σ_{yo}, are a drag stress and initial yield stress at a stabilized hysteretic behavior. C_k, γ_k, b, and Q are the material parameters to be identified in this study, which come from the kinematic and isotropic hardening models.

There are typically two types of material hardening behavior when stress state exceeds the elastic limit. One type is a kinematic hardening behavior representing the yield surface translation in deviatoric stress space. Another one is an isotropic hardening behavior representing the expansion of the yield surface without translation. The material hardening behavior can occur with one of two types or both.

2.1.1. Kinematic Hardening Model

For the kinematic hardening rule, Chaboche model with deviatoric backstresses is expressed as follows [17–19]:

$$\dot{\alpha} = \sum_{k=1}^{m} \left(\frac{2}{3} C_k \dot{\varepsilon}^p - \gamma_k \alpha_k \dot{p} \right) \tag{6}$$

where C_k and γ_k are material parameters to be identified and $\dot{p}$ is the magnitude of plastic strain tensor $(=\left|\dot{\varepsilon}^p\right|)$.

2.1.2. Isotropic Hardening Model

For the isotropic hardening rule, the Voce model is used as follows [20]:

$$\dot{R} = b[Q - R]\dot{p} \tag{7}$$

where b and Q are material parameters to be identified. When the initial value $R = 0$, integrating Equation (7) gives:

$$R = Q\left(1 - e^{-bp}\right) \tag{8}$$

2.2. Unified Viscoplastic Model

The total strain tensor ε_t can be expressed by the sum of the separate elastic strain (ε_e), plastic strain (ε_p), and viscous (creep) strain (ε_v), as follows:

$$\varepsilon_t = \varepsilon_e + \varepsilon_p + \varepsilon_v \tag{9}$$

In the above equation, the plastic strain and viscous strain can be summed and expressed as the viscoplastic strain ε_{vp}. And the total strain tensor can be rewritten as follows;

$$\varepsilon_t = \varepsilon_e + \varepsilon_{vp} \tag{10}$$

In Equation (10), the elastic strain, ε_e can be obtained by Hooke's as follows:

$$\varepsilon_e = \frac{1+\nu}{E}\sigma - \frac{v}{E}(tr\sigma)I \tag{11}$$

where E, σ, ν, tr, and I are Young's modulus, the stress tensor, Poisson's ratio, the trace, and unit tensor of second-rank respectively. The inelastic strain rate equation of the unified Chaboche's model is used for the viscoplastic strain as follows [16–19]:

$$\dot{\varepsilon}_{vp} = \frac{3}{2}\dot{p}\frac{\tau - \alpha}{J(\sigma - a)} \tag{12}$$

where $(\cdot)$ indicates a differentiation by time. a, τ, and α are the total back stress tensor, the deviator of the stress tensor, and the deviatoric back stress tensor of Equation (6), respectively. The $\dot{p}$ indicates an evolution of the accumulated inelastic strain expressed by

$$\dot{p} = \left\langle \frac{J(\sigma - a) - R}{K} \right\rangle^n \tag{13}$$

where K and n are material parameters related with the viscous behavior and R is a drag stress as presented in Equation (8). The symbol of < > indicates the McCauley bracket ($<x> = 0$ if $x < 0$; $<x> = x$ if $x \geq 0$). The von Mises distance in the deviatoric stress space J can be expressed as follows;

$$J(\sigma - a) = \left[\frac{3}{2}(\tau - \alpha)\bullet(\tau - \alpha)\right]^{1/2} \tag{14}$$

where the symbol of • means the inner product as $x \bullet y = x_{ij}y_{ij}$.

The following explicit time integration of the rate of the state variables produces the inelastic strain, back stress, and drag stress at time t_{k+1}:

$$\sigma(k) = E\left[\varepsilon(k) - \varepsilon_{vp}(k)\right] \tag{15}$$

$$\varepsilon_{vp}(k) = \varepsilon_{vp}(k-1) + \Delta t \cdot \dot{\varepsilon}_{vp}(k-1) \tag{16}$$

$$\alpha(k) = \alpha(k-1) + \Delta t \cdot \dot{\alpha}(k-1) \tag{17}$$

$$R(k) = R(k-1) + \Delta t \cdot \dot{R}(k-1) \tag{18}$$

3. Tests for Parameter Identifications

In order to identify the material parameters required in Equations (6)–(8) and (13), various test data are required from specimen tests as follows;

- Uniaxial tension data (yield stress);
- Strain-controlled stabilized hysteresis loop data (kinematic hardening parameters);
- Strain-controlled cyclic hysteresis loop data (isotropic hardening parameters);
- Stress relaxation data (viscous parameters);
- Stress-controlled ratcheting data (ratchet parameters).

Figure 1 shows the photos of the test facility and specimens used. The test facility consists of MTS hydraulic actuator, a 3-zone controlled electric heat furnace, hydraulic grip, alignment fixture, and the extensometer. The gage length of the specimen is 15 mm, and the test sectional diameter is 6 mm, which are in compliance with the ASTM E466 requirement.

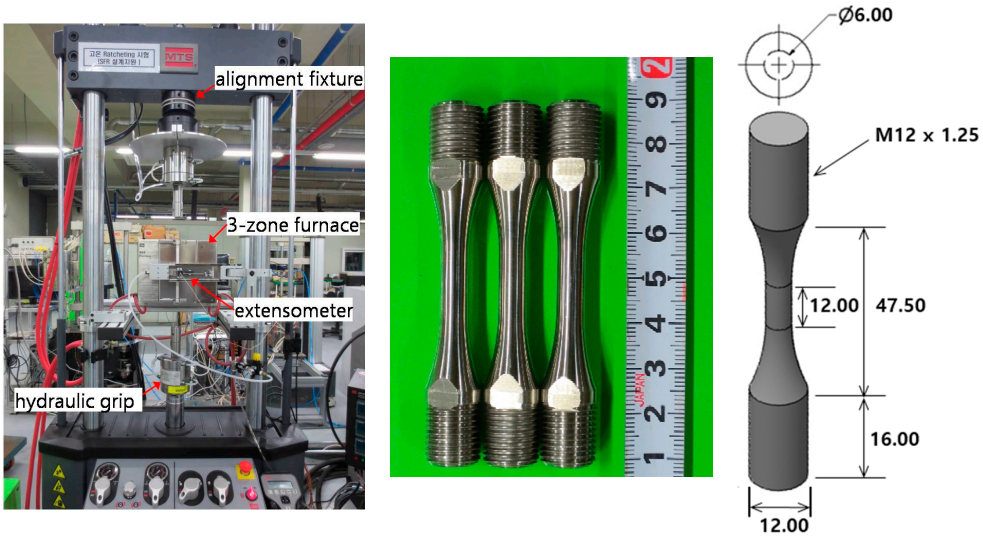

(**a**) (**b**) (**c**)

Figure 1. Photos of test facility and specimen used: (**a**) facility; (**b**) specimen; (**c**) schematics and dimensions of specimen.

Table 1 presents the chemical compositions of Type 316H used for the specimen.

Table 1. Chemical compositions of Type 316H used in the study (wt%).

Cr	Ni	Mo	Mn	Si	Cu	P	S	C	N	Fe
16.26	10.16	2.05	1.76	0.44	0.48	0.034	0.001	0.05	0.05	Val.

3.1. Uniaxial Tension Data

As typical characteristics of an austenitic stainless steel, the Type 316H stainless steel revealed a dynamic strain aging (DSA) behavior in tension tests, which is an instability in the plastic flow of materials associated with interaction between moving dislocations and diffusing solutes. Figure 2 shows the tension test results for the isothermal condition of specific elevated temperatures. In this figure, we can see the manifestation of type A and type B serration, which indicate DSA phenomena [21]. We can also see that the DSA occurs at some specific strain rate as shown in Figure 3. Actually, the initial strains are all the same as zero. The curves in Figures 2 and 3 are intentionally moved a little to avoid overlapping curves and to show the DSA phenomena clearly.

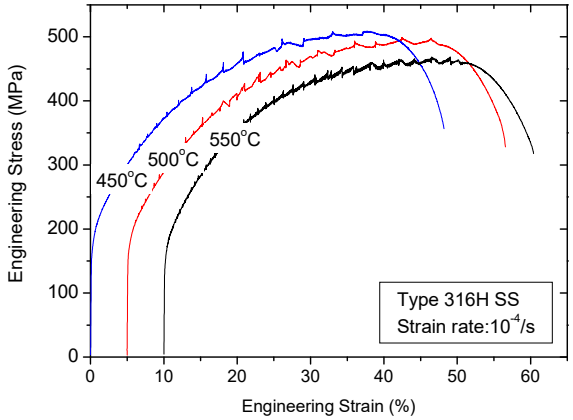

Figure 2. Results of tension tests.

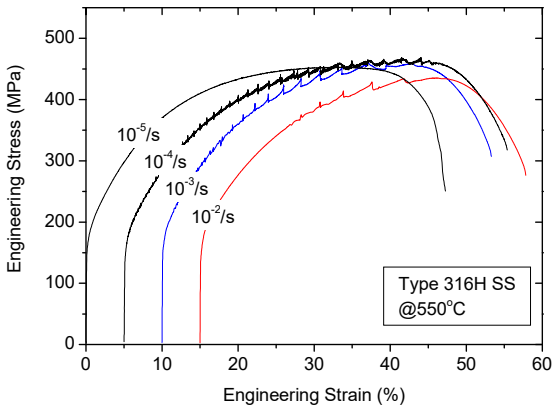

Figure 3. Results of tension tests with various strain rates at 550 °C.

3.2. Strain-Controlled Cyclic Hysteresis Loop Data

To obtain the material parameters for the kinematic and isotropic hardening models in Equations (6) and (8), the strain-controlled cyclic tests are carried out with a fully reversed total strain range of 1.2% (±0.6%) and a constant strain rate of 1×10^{-4}/s.

Figure 4 presents the test results of the cyclic hysteresis behavior for various isothermal conditions from room temperature (RT) to 650 °C.

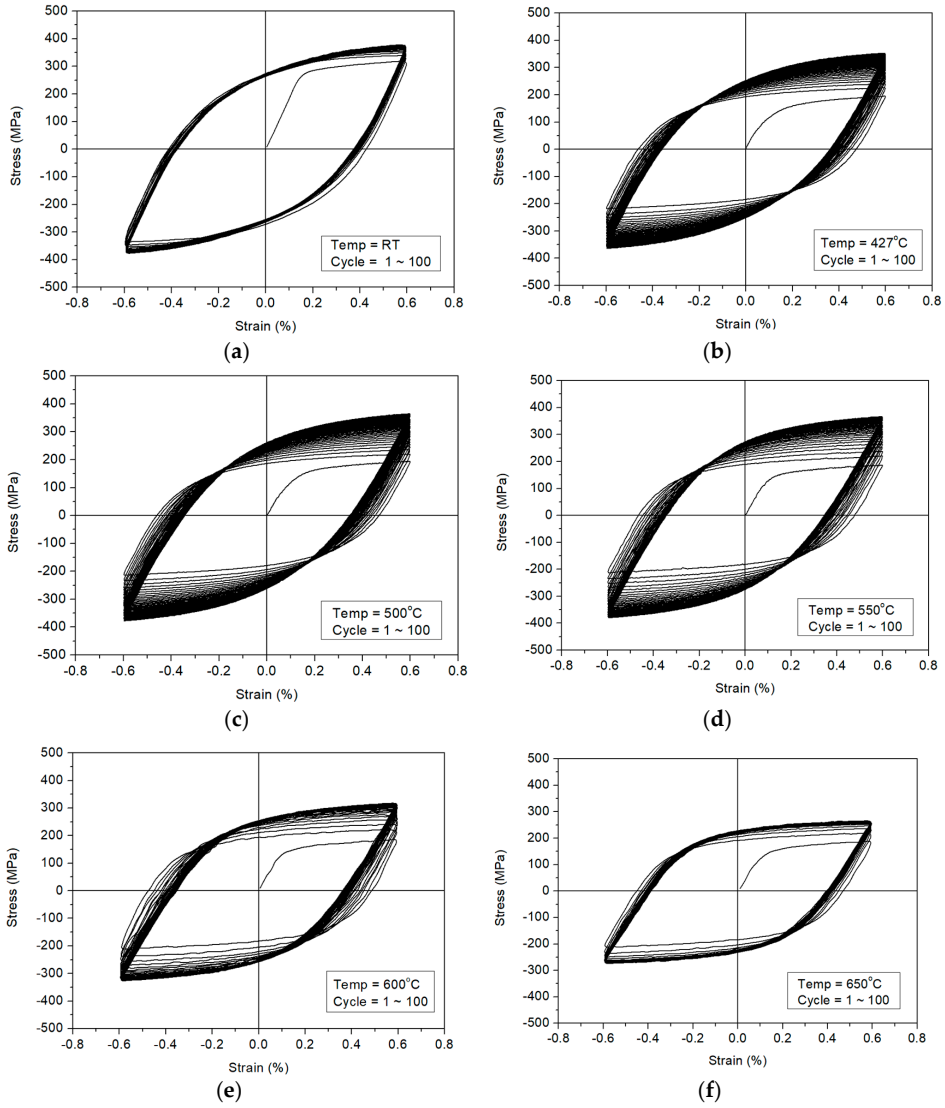

Figure 4. Test results of cyclic hysteresis loops: (**a**) Room Temperature (RT); (**b**) 427 °C; (**c**) 500 °C; (**d**) 550 °C; (**e**) 600 °C; (**f**) 650 °C.

As shown in Figure 4, Type 316H material is quickly stabilized at RT and over 600 °C with a lower number of cycles compared with those of temperature ranges from 427 to 600 °C, which reveals DSA phenomena.

Figure 5 presents the test data of the stabilized hysteresis loops of the stress–strain curves for each isothermal conditions from room temperature (RT) to 650 °C corresponding to 100th cycle selected in Figure 4.

As shown in Figure 5, the maximum peak stresses at temperature of 500 °C and 550 °C are slightly larger than those at room temperature and 425 °C due to the DSA phenomena. For a higher temperature range, over 600 °C, the maximum stress significantly reduced compared with those of the lower temperatures.

Figure 6 shows the maximum hardening ratio (i.e., max. peak stress/initial peak stress) for each isothermal condition. As shown in the figure, the hardening ratio is relatively larger at specific temperatures from 500 °C to 575 °C due to DSA effects. The test specimens used in this study were machined from a Type 316H plate fully solution annealed at 1050 °C for one hour. However, the thermal solute strength effect may be expected to be apparent at abnormal temperature ranges. Therefore, more detailed investigations are needed for the solute effects.

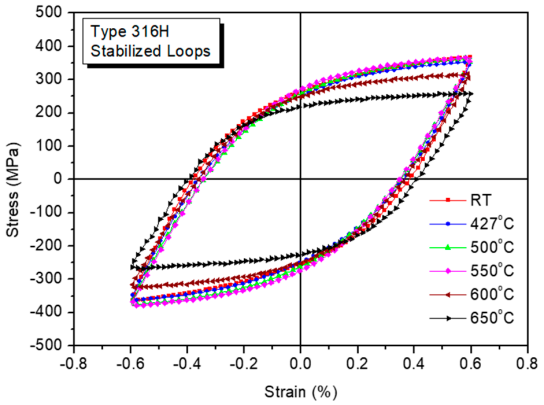

Figure 5. Stabilized hysteresis loops at 100th cycle.

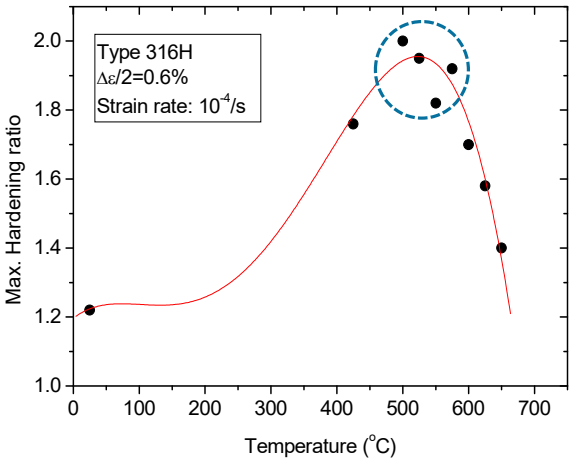

Figure 6. Cyclic hardening behavior.

4. Identification of Material Parameters

4.1. Elasto-Plastic Model

In this paper, the three decomposed rule (m = 3) of the evolution of the deviatoric backstress, $\dot{\alpha}$ in Equation (6), is used for the kinematic hardening material model. This model requires that the first back stress, α_1 should be set to have a sufficently large modulus value at the beginning of the hardening behavior, and should stabilize quickly. The second back stress, α_2 should be identified to describe the transient nonlinear part. The third back stress, α_3 should be identified to describe the linear hardening behavior of the hysteresis loop throughout all strain ranges. The material parameters of C_1, C_2, C_3 and γ_1, γ_2, γ_3 in the three backstresses can be identified from the test results of the stabilized stress–strain cyclic behavior. In this identification method, the C_1 should have a very large value matching the plastic modulus at yielding and γ_1 should be a sufficiently large value to stabilize the kinematic hardening of α_1. The C_3 parameter should be determined to be the slope of the linear segment of the hysteresis loop at a high strain range. The C_2 and γ_2 parameters should be determined by trials in satisfying the specific relationship at or near the plastic strain limit [22]. The parameter γ_3 represents the ratchet parameter. This can be determined through ratchet tests with various mean stress conditions.

For the isotropic hardening model, the material parameters of b and Q in Equation (8) should be identified to be able to express the maximum stress at each cycle.

Table 1 presents the material parameters identified for the elastic–plastic constitutive equation using the Chaboche model with three backstresses for the kinematic hardening behavior and Voce model for the isotropic hardening behavior.

Figure 7 presents the comparison results of the strain-controlled cyclic behavior between calculations of the elasto-plastic material model using the material parameters of Table 2 and test results of Figure 4 for each isothermal condition.

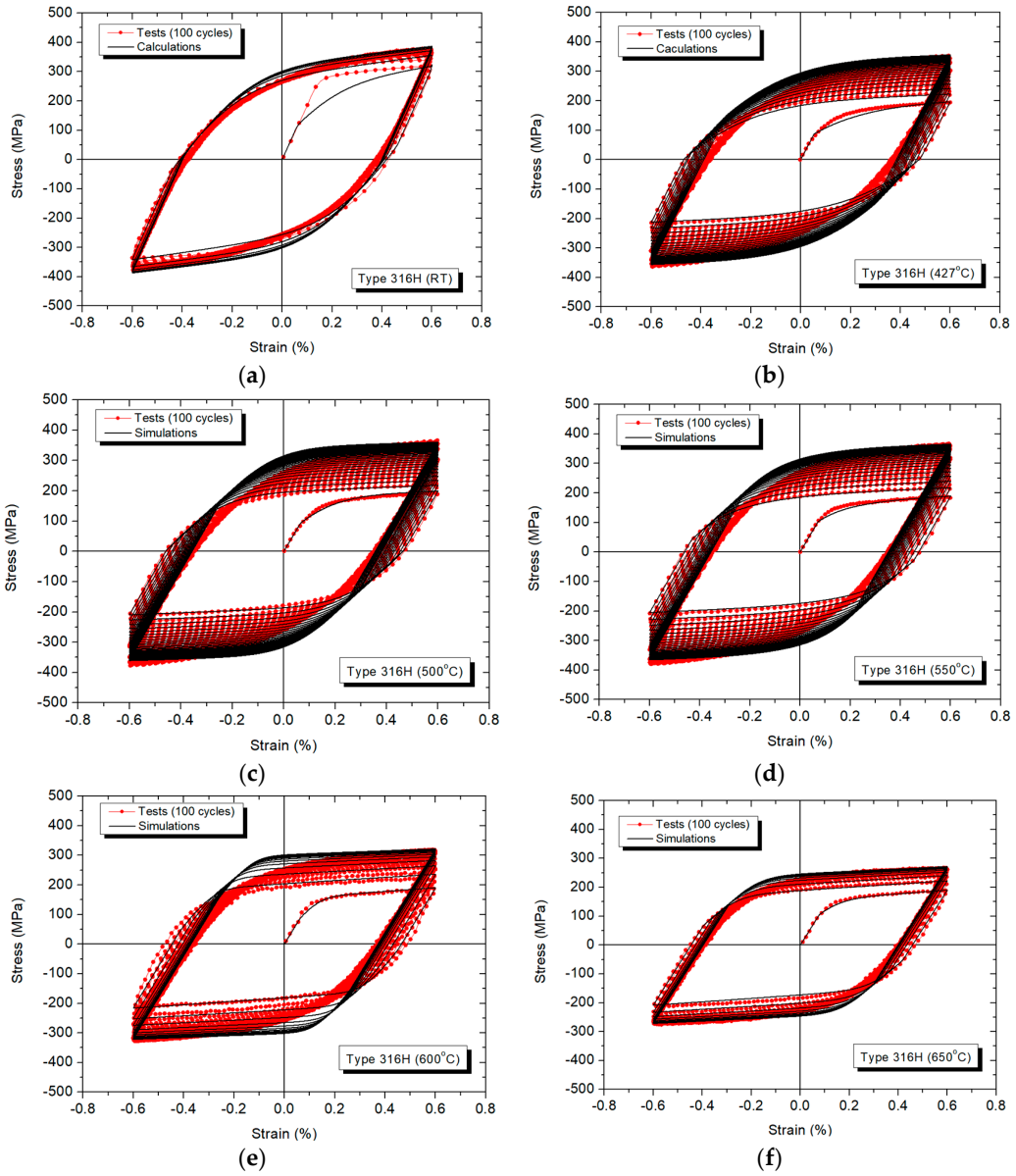

Figure 7. Comparison of strain-controlled cyclic behavior between tests and calculation results of the elasto-plastic material model: (**a**) RT; (**b**) 427 °C; (**c**) 500 °C; (**d**) 550 °C; (**e**) 600 °C; (**f**) 650 °C.

Table 2. Identified Material Parameters for Elasto-Plastic Model.

Temp (°C)	σ_{yo} (MPa)	E (GPa)	C_1 $\times 10^9$	C_2 $\times 10^9$	C_3 $\times 10^9$	γ_1 $\times 10^3$	γ_2 $\times 10^3$	γ_3	b	Q $\times 10^6$
RT	135	190	120	20.20	10.670	1.0	1.00	1.0	45.0	85
427	86	170	80	14.02	3.333	0.9	1.50	1.0	12.0	165
500	90	150	6	163.3	3.333	0.9	1.87	1.0	10.0	170
550	100	150	40	91.62	3.333	0.9	3.10	1.0	13.0	185
600	105	140	160	3.48	6.333	3.0	5.50	1.0	23.7	150
650	105	136	161	1.65	6.333	3.0	5.50	1.0	42.0	96

As presented in Figure 7, we can see that the material parameters for the elasto-plastic material model proposed in Table 2 can accurately express the cyclic hardening behavior for each cycle.

To identify the ratcheting parameter, γ_3, the uniaxial ratcheting tests are carried out by the stress-controlled test procedures with various mean stress conditions. Figure 8 presents the ratcheting test results for each isothermal condition with stress amplitude of 150 MPa, mean stress of 50 MPa, and stress rate 5 MPa/s. As shown in the figure, Type 316H stainless steel reveals a stabilization to plastic shakedown after a few cycles without ratcheting behavior. Especially at a higher temperature of 650 °C, Type 316H reveals an apparent kinematic hardening behavior with more accumulation of a cyclic plastic strain, but finally reaches plastic shakedown after a few cycles without ratcheting.

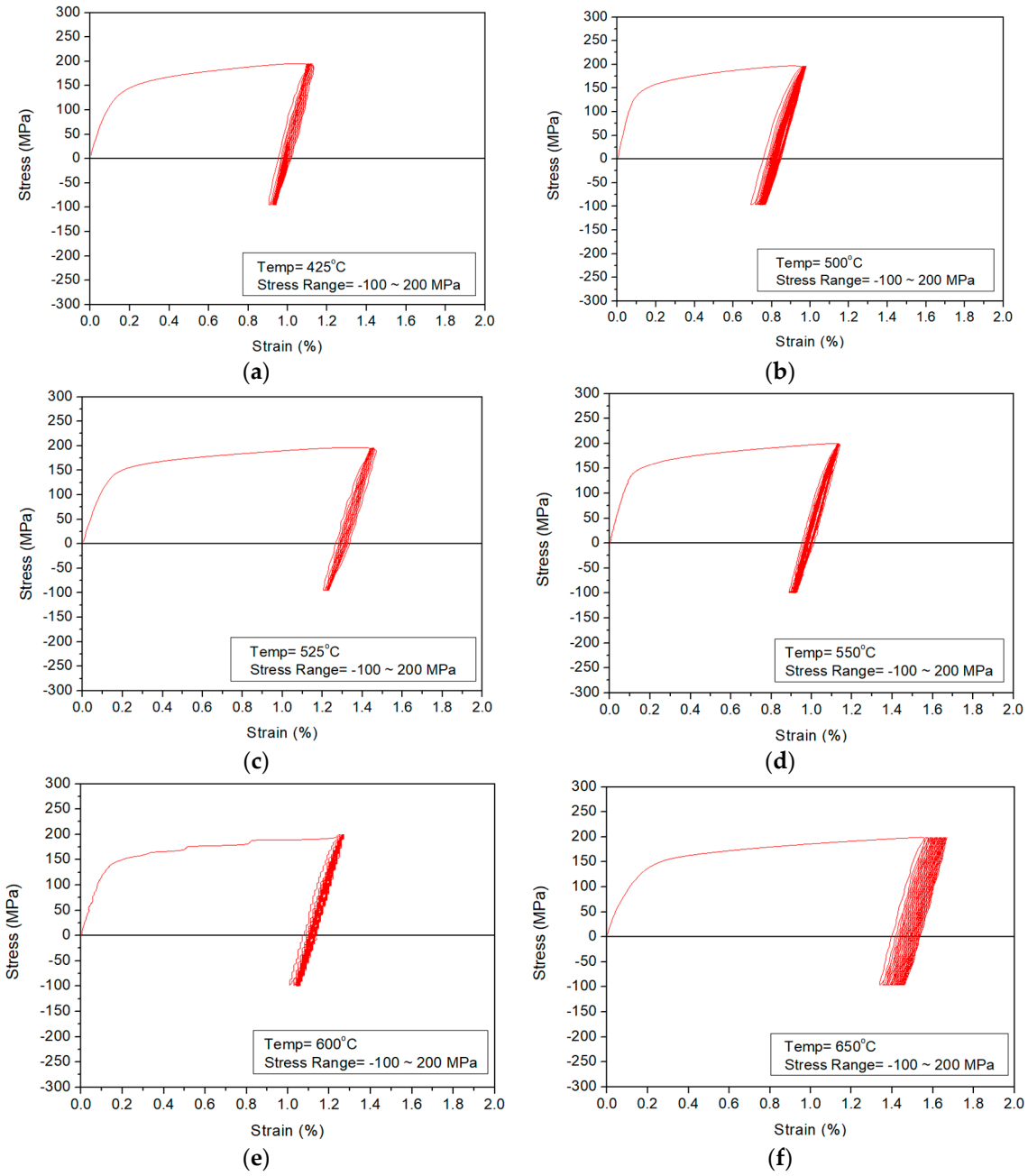

Figure 8. Test results of ratcheting (stress rate: 5 MPa): (**a**) 425 °C; (**b**) 500 °C; (**c**) 525 °C; (**d**) 550 °C; (**e**) 600 °C; (**f**) 650 °C.

To investigate the effects of stress amplitudes and the mean stress levels in ratcheting, the stress-controlled cyclic tests with different stress levels were carried out at 550 °C. Figure 9 presents the test results for two cases; stress amplitude of 150 MPa with a mean stress of 50 MPa, stress amplitude of 220 MPa with a mean stress 30 MPa.

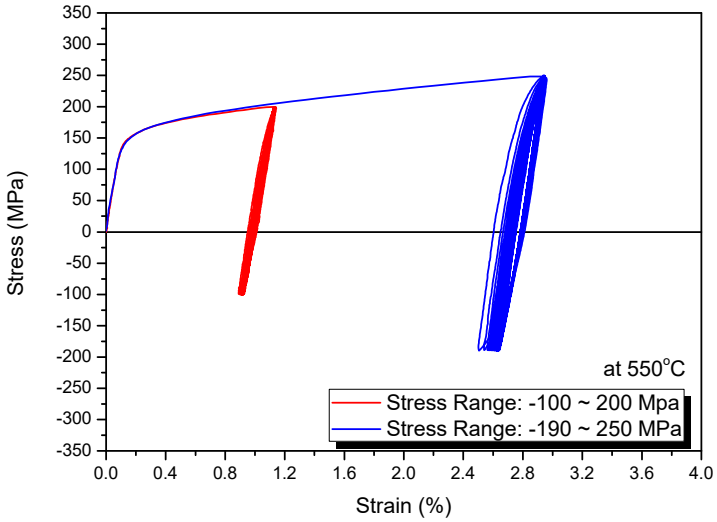

Figure 9. Test results of ratcheting at 550 °C with different stress conditions (stress rate: 5 MPa/s).

As shown in Figure 9, we can see that the plastic shakedown occurred for both conditions after a few cycles without ratcheting behavior.

4.2. Unified Viscoplastic Model

The Table 1, which presents the kinematic and isotropic hardening parameters for the elasto-plastic model, is also used for the unified viscoplastic material model. To express the time dependent material behavior, Table 3 presents the additional material parameters required for the unified viscoplastic model in Equation (13).

Table 3. Identified Material Parameters for Unified Viscoplastic Model.

Temp. (°C)	$K \times 10^6$	n
RT	-	-
427	91	50
500	102	41
550	150	18
600	125	17
650	340	7

To validate the material parameters of Tables 2 and 3 for the unified viscoplastic model of Equations (9)–(18), the strain-controlled cyclic calculations were carried out and the results are compared with the test data. Figure 10 shows the comparison results for each isothermal condition.

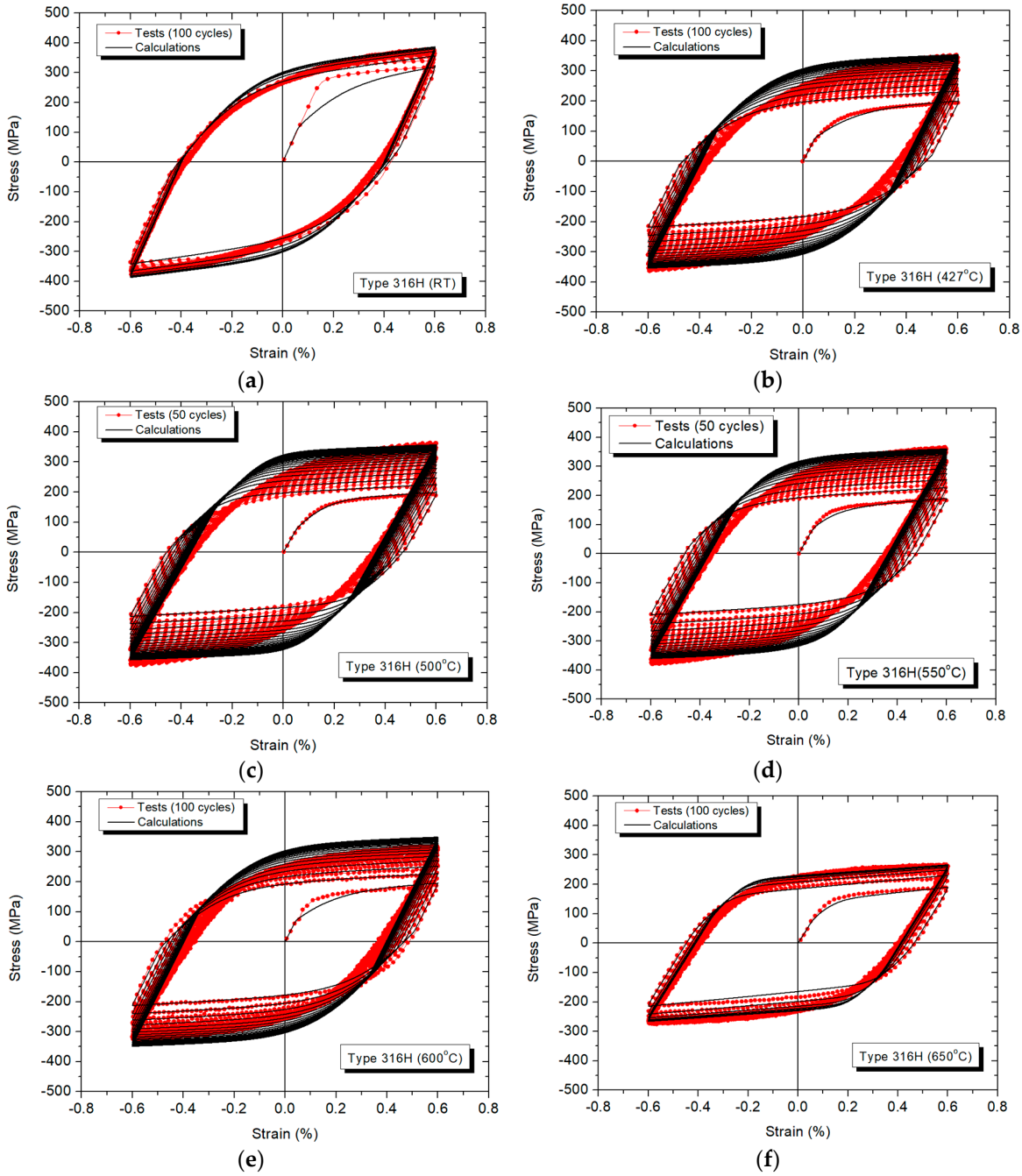

Figure 10. Comparison of cyclic hysteresis loops between tests and calculation results of the unified viscoplastic material model: (**a**) RT; (**b**) 427 °C; (**c**) 500 °C; (**d**) 550 °C; (**e**) 600 °C; (**f**) 650 °C.

As shown in Figure 10, we can see that the calculation results of the unified viscoplastic model give a good agreement with the test results in strain-controlled cyclic behavior.

To see the time dependent material behavior of Type 316H, the stress relaxations are calculated for a hold strain level of 0.6% and a loading strain rate of 8.3×10^{-5} (1/s). Figure 11 presents the calculation results of the stress relaxation for each isothermal condition and they are compared with the stress relaxation data obtained from the Isochronous stress–strain curves (ISSC) in the ASME-Division 5 Nonmadatory Appendix HBB-T.

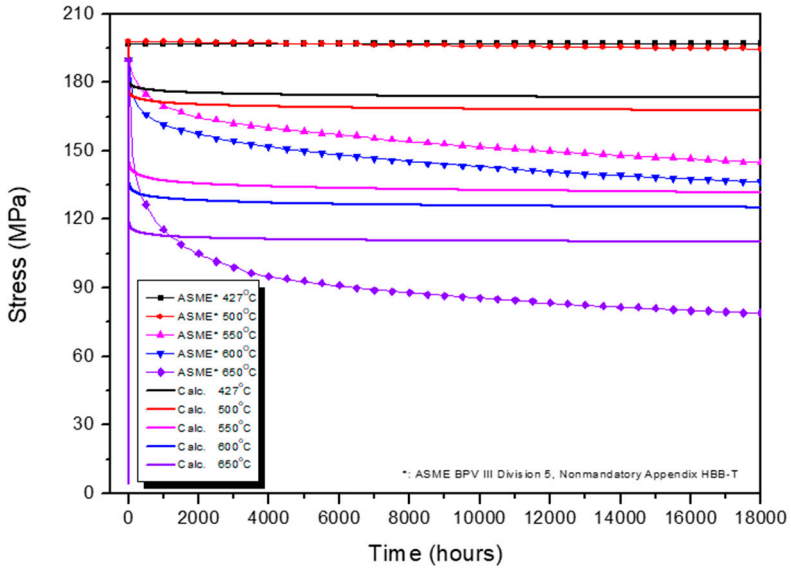

Figure 11. Calculation results of stress relaxation.

As shown in Figure 11, the overall calculated values reveal more rapid stress relaxation behavior during initial time than those of ASME data. At the temperatures less than 500 °C, the stress relaxation is almost negligible, and the stress relaxation strengths seem to be constant at least up to 18,000 h. We can see that the overall trend of stress relaxations at 550 °C and 600 °C is similar but significant stress relaxation occurs at an elevated temperature of 650 °C. The calculation results using the material parameters of Table 3 reveal some discrepancies with those of the ASME stress relaxation data, but give appropriate engineering predictions of stress relaxation from the point of view of using the least material parameters.

5. Conclusions

In this paper, the inelastic material models for Type 316H, which is one of principal candidate materials for elevated temperature design of the HTRs components, are investigated and the required number of material parameters are simplified to be ten for the elasto-plastic model, with an additional two for the unified viscoplastic model.

From the material tests of the Type 316H, we can see that the dynamic strain aging effects significantly occur around 500–550 °C and the identified inelastic material parameters are not consistent at that temperature range. However, it is recommended that the interpolation can be applied to all parameters identified at 50 °C intervals. Related to the ratcheting material parameters, γ_3 is set to be 1.0 for all specified temperature ranges because the ratcheting behavior is not detected in design level stress-controlled cyclic tests.

Through the comparison study, it is found that the calculation results of inelastic material behavior, such as stabilized cyclic stress–strain curve, cyclic hardening, and stress relaxations are in a good agreement with those of tests. Therefore, it is expected that the identified material parameters for the elasto-plastic and the viscoplastic material models of the Type 316H are available for an inelastic analysis of the HTRs components at elevated temperature service.

Author Contributions: Conceptualization, G.-H.K.; data curation, J.-H.Y.; writing—original draft preparation, G.-H.K.; writing—review and editing, J.-H.Y.; project administration, G.-H.K.; funding acquisition, G.-H.K. All authors have read and agreed to the published version of the manuscript.

Funding: This study was funded by the Ministry of Trade, Industry and Energy through Korea Institute of Energy Technology Evaluation Planning (KETEP) (No. 20181510102380).

Conflicts of Interest: The authors declare no conflict of interest.

References

1. ASME. *ASME Boiler and Pressure Vessel Code Section III*; Division 5; ASME: New York, NY, USA, 2019.
2. AFCEN. *RCC-MRx: Design and Construction Rules for Mechanical Components in High-Temperature Structures, Experimental Reactors, Fusion Reactor*; AFCEN: Lyon, France, 2015.
3. PNC. *Elevated Temperature Structural Design Guide for Class 1 Components of Prototype Fast Breeder Reactor*; PNC N241-84-08; PNC: Yokohama, Japan, 1984.
4. British Energy Generation Ltd. *Assessment Procedure for the High Temperature Response of Structures*; British Energy Generation Ltd.: Gloucester, UK, 2003.
5. Messner, M.C.; Sham, T.L. Isochronous stress-strain curves for Alloy 617. In Proceedings of the ASME 2019 Pressure Vessels & Piping Conference, San Antonio, TX, USA, 14–19 July 2019.
6. Bonne, D.; Dubiez-LeGoff, S.; Drubay, B. Codification of 316LN in RCC-MR code: Experience and prospective projects. In Proceedings of the ASME 2010 Pressure Vessels and Piping Conference, Bellevue, WA, USA, 18–22 July 2010.
7. Esposito, L.; Bonora, N.; Vita, G.D. Creep modelling of 316H stainless steel over a wide range of stress. *Procedia Struct. Integr.* **2016**, *2*, 927–933. [CrossRef]
8. Phan, V.-T.; Messner, M.C.; Sham, T.-L. A unified engineering inelastic model for 316H stainless steel. In Proceedings of the ASME 2019 Pressure Vessels & Piping Conference, San Antonio, TX, USA, 14–19 July 2019.
9. Li, X.; Holdsworth, S.R.; Mazza, E.; Hosseini, E. Creep behavior of AISI 316H stainless steel under stress-varying creep loading conditions: Primary creep regeneration. *J. Mater. High Temp.* **2019**, *36*, 240–252. [CrossRef]
10. Shimada, T.; Tokuda, K.; Yoshida, K.; Ohno, N.; Sasaki, T. Creep-fatigue life prediction of 316H stainless steel by utilizing non-unified constitutive model. *Procedia Struct. Integr.* **2018**, *13*, 1873–1878. [CrossRef]
11. Petkov, M.P.; Hu, J.; Cocks, C.F. Self-consistent modelling of cyclic loading and relaxation in austenitic 316H stainless steel. *J. Philos. Mag.* **2019**, *99*, 789–834. [CrossRef]
12. Wang, Y.Q.; Spindler, M.W.; Truman, C.E.; Smith, D.J. Critical analysis of the prediction of stress relaxation from forward creep of Type 316H austenitic stainless steel. *Mater. Des.* **2016**, *95*, 656–668. [CrossRef]
13. Youtsos, A.G.; Donea, J.; Verzeletti, G.; Italy, I. Viscoplastic behavior of stainless steels AISI 316L and 316H. *Acta Mech.* **1989**, *76*, 161–187. [CrossRef]
14. Albertini, C.; Montagnani, M.; Micunovic, M. Viscoplastic behavior of AISI 316H: Multiaxial experimental results and preliminary numerical analysis. *Nucl. Eng. Des.* **1991**, *130*, 205–210. [CrossRef]
15. Koo, G.H.; Lee, J.H. Investigation of ratcheting characteristics of modified 9Cr-1Mo steel by using the chaboche constitutive model. *Int. J. Press. Vessel. Pip.* **2007**, *84*, 284–292. [CrossRef]
16. Koo, G.H.; Kwon, J.H. Identification of inelastic material parameters for modified 9Cr-1Mo steel applicable to the plastic and viscoplastic constitutive equations. *Int. J. Press. Vessel. Pip.* **2011**, *88*, 26–33. [CrossRef]
17. Chaboche, J.L.; Rousselier, G. On the plastic and viscoplastic constitutive equations—Part I: Rules developed with internal variable concept. *J. Press. Vessel. Technol.* **1983**, *105*, 153–158. [CrossRef]
18. Chaboche, J.L.; Rousselier, G. On the plastic and viscoplastic constitutive equations—Part II: Application of internal variable concepts to the 316 stainless steel. *J. Press. Vessel. Technol.* **1983**, *105*, 159–164. [CrossRef]
19. Chaboche, J.L. Constitutive equations for cyclic plasticity and cyclic viscoplasticity. *Int. J. Plast.* **1989**, *5*, 247–302. [CrossRef]
20. Voce, E. A practical strain-hardening function. *Metallurgia* **1955**, *51*, 219–225.
21. Armas, A.F.; Bettin, O.R.; Alvarez-Armas, I.; Rubiolo, G.H. Strain aging effects on the cyclic behavior of austenitic stainless steel. *J. Nucl. Mater.* **1988**, *155*, 646–649. [CrossRef]
22. Bari, S.; Hassan, T. Anatomy of coupled constitutive models for ratcheting simulation. *Int. J. Plast.* **2000**, *16*, 381–409. [CrossRef]